remote sensing

MDPI

Article

Terrestrial Photogrammetry–GIS Methodology for Measuring Rill Erosion at the Sparacia Experimental Area, Sicily

Vincenzo Palmeri [1,2], Costanza Di Stefano [1], Alessio Nicosia [1,*], Vincenzo Pampalone [1] and Vito Ferro [1,2]

[1] Department of Agricultural, Food and Forest Sciences, University of Palermo, Viale delle Scienze, 90128 Palermo, Italy; vincenzo.palmeri02@unipa.it (V.P.); costanza.distefano@unipa.it (C.D.S.); vincenzo.pampalone@unipa.it (V.P.); vito.ferro@unipa.it (V.F.)

[2] NBFC, National Biodiversity Future Center, 90133 Palermo, Italy

* Correspondence: alessio.nicosia@unipa.it

Abstract: Rill erosion is a major issue on a global scale, and predicting the presence, position, and development of erosive forms on hillslopes is a significant challenge for the scientific community. Several plot-scale investigations confirmed the reliability of the terrestrial photogrammetric (TP) technique for studying rill erosion and the reliability of a method for extracting the rill network from Digital Surface Models (DSMs) and measuring the corresponding volume. In this paper, for an intense erosive event that occurred at the Sparacia experimental area (Sicily, Southern Italy), TP surveys of three plots, with different length and steepness, incised by rills, were performed to reconstruct the DSMs. For each plot, the rill network was extracted from the DSMs, and the non-contributing network was distinguished from the contributing one, from which the soil loss and the consequent eroded volumes V were determined. The specific aims were to (i) establish the effect of plot steepness on rill depths and some morphometric characteristics of the drainage rill network; (ii) test and calibrate the relationship between V and the total rill length L, using all rill measurements available in the literature and those obtained in this study; and (iii) modify the V–L relationship by including climate forcing and assessing the related performance. The rill depths, h, the drainage frequency, and drainage density of the rill networks detected in the three plots were compared. The analysis demonstrated that h and the morphometric parameters of the contributing rill network increase with plot steepness s. In particular, the mean depth increases from 2.79 to 4.85 cm for slope increasing from 14.9 to 26%. Moreover, the drainage frequency of the contributing rill network varies from 0.16 m^{-2} for s = 14.9% to 0.47 m^{-2} for s = 26%, while the drainage density of the contributing rill network varies from 0.92 m^{-1} for s = 14.9% to 2.1 m^{-1} for s = 26%. Finally, using the data available in the literature and those obtained in this investigation, an empirical relationship between V and the total rill length L was firstly tested and then rearranged considering the event rainfall erosivity R_e. Including R_e in the rearranged equation guaranteed the best performance in V estimation.

Keywords: soil loss; rainfall; rill erosion; close-range photogrammetry

Citation: Palmeri, V.; Di Stefano, C.; Nicosia, A.; Pampalone, V.; Ferro, V. Terrestrial Photogrammetry–GIS Methodology for Measuring Rill Erosion at the Sparacia Experimental Area, Sicily. *Remote Sens.* **2024**, *16*, 4232. https://doi.org/10.3390/rs16224232

Academic Editor: Jorge Delgado García

Received: 27 September 2024
Revised: 7 November 2024
Accepted: 12 November 2024
Published: 13 November 2024

1. Introduction

Predicting the presence, position, as well as development of erosive formations on hillslopes and agricultural landscapes continues to be an important difficulty in land management, as soil erosion by water is a major issue on a global scale [1]. Shi et al. [2] found that the hillslope erosion goes through five evolutionary stages (i.e., inter-rill erosion, rill development, stabilized rill, ephemeral gully development, and stabilized ephemeral gully), which are characterized by changes in sediment load, channel morphology, hydraulic parameters, and particle size distribution. Rill erosion is an important form of hillslope soil erosion that occurs by overland flow at the steep slopes [3]. In these conditions, runoff tends to concentrate in narrow channels (water depths varying from the order of millimeters to several centimeters), named rills [4], whose geometry is dependent on surface roughness,

topographic irregularities, and tillage operations. For intense rainfall events, rills often develop, and the contribution of rill erosion to total soil loss is generally dominant [1]. In particular, according to the literature [5–7], approximately 80% of erosion at the hillslope scale is due to the rill component. When additional shear stresses of channelized flows cause soil particle detachment from the rill boundaries, rills gradually enlarge until they become ephemeral gullies (EGs) [8]. The rill networks develop in complex ways, and the rill morphology can contribute to the uncertainty and complexity of the main processes of rill development. Measurements of rill morphology include cross-section size, rill network length, and number of rills [9]. The rill network can be detected using direct and indirect methods. The former is time-consuming and can produce alteration of the rilled area because of the passage of the operator. The latter, including three-dimensional (3D) photo-reconstruction techniques and the terrestrial laser scanner [10,11], overcomes these troubles and generates accurate 3D models. Recently, several plot-scale investigations [12–15] demonstrated the reliability of the terrestrial photogrammetric technique for rill survey. Gessesse et al. [12] surveyed, using a calibrated non-metric digital camera (Canon EOS 1Ds), a rilled plot subjected to extreme rainfall events, demonstrating that the DEM measurements led to a relative error of $\pm$2.8 to $\pm$5.3 mm, detecting erosion and deposition. Di Stefano et al. [13] positively tested the applicability of the Structure from Motion (SfM) for rill channels shaped in a plot, comparing the measurements (surface width, maximum depth, cross-section area, perimeter, and hydraulic radius), in 11 cross-sections, obtained by a 6 m long gypsum cast of the rill and those obtained with the 3D model generated by photos acquired with a GoPro Hero 4 Silver (© 2024 GoPro Inc., San Mateo, CA, USA) camera. Moreover, the reliability of this model for measuring rill erosion was confirmed by the satisfying results obtained by comparing, for three rills, the sediment weight transported by the rill flow and collected in a storage tank at the outlet of the plot with that obtained by converting the eroded volume obtained by the DEM of difference (i.e., the difference between the 3D model of the initial condition and that of the final one). Jiang et al. [14] tested a digital close-range photogrammetric observation system combined with a GIS methodology to monitor the morphological development of rill erosion, extracting rill networks and obtaining the main parameters of the rill erosion (rill density, average rill depth, etc.). These authors, comparing the soil loss values obtained by the traditional method and those obtained by close-range photogrammetry, also found a high estimation precision, which increases with the rainfall duration. The same methodology was also used by Jiang et al. [15], who applied close-range photogrammetry and a GIS methodology to compare the responses of two different soils to rill erosion processes.

Different methods exist for the extraction of a channel network from a Digital Surface Model (DSM), such as the Canny operator [16], slope analysis [11], Broscoe's method [17], landform curvature [18,19], and that combining the convergence index and a drainage algorithm [20]. Several experimental investigations distinguished between contributing rills, belonging to the network connected to the plot outlet and contributing to the soil loss measured there, and non-contributing rills, whose interruption within the plot prevents them from contributing to soil loss. This distinction allows for improving the accuracy of the eroded volume measurement. Gessesse et al. [12] used an approach based on the application of close-range digital photogrammetry to survey microtopographic soil surface changes caused by erosion and investigate sediment transport in inter-rill and rill areas and rill erosion for a rainfall event. The authors found that an abrupt change in surface microtopography controls the rill network. In particular, rough surfaces are characterized by many smaller rills, but fewer contributing rills as compared to relatively smooth surfaces. Di Stefano et al. [20] performed both terrestrial and low-altitude aerial surveys after an erosive event occurred at the Sparacia experimental area (Southern Italy) to measure rill erosion on two plots. These authors, for the first time, extracted the rill network, applying the convergence index to high-resolution rill data, and then distinguished contributing and non-contributing rills, developing an automatic approach detailed below. The results denoted a better capability of the terrestrial survey in detecting rills and highlighted that,

on average, contributing rills are longer than non-contributing ones and their measurement is independent of the data acquisition platform. For a natural erosive event monitored on a plot of the Sparacia (Sicily) experimental area, Carollo et al. [21] measured geometric variables of rills and calculated network morphometric indexes. In addition, they positively tested the reliability of an automatic method [20], which applies the convergence index and a threshold value L_T that identifies the rill interruption length, to distinguish between non-contributing and contributing rills.

Despite past efforts, much work is still to be conducted concerning the measurement and modeling of rill erosion and upscaling from plot to natural hillslope. Accurate and repeatable rill erosion measurements need both for correct modeling [13].

Physically based and process-oriented erosion models suffer from uncertainty due to many input parameters to be measured or estimated. This circumstance induced researchers to propose simple empirical relationships to estimate the channelized erosion [22]. Rejman and Brodowski [23] surveyed rills on plots with different lengths and found a linear relationship of the total rill volume versus plot length. Nachtergaele et al. [24], using EG measurements at the event scale, and Capra et al. [25], using rill measurements at the event scale and EG data collected annually (i.e., all rainfall events during the wet period) or for each rainfall erosive event, suggested that the channel volume V can be estimated simply using its length, L, with the following equation:

$$V = aL^b \quad (1)$$

where a and b are numerical coefficients.

Bruno et al. [22], using rill measurements performed for five events at Sparacia, established a = 0.0038 and b = 1.16. Di Stefano and Ferro [26], using 269 rill measurements carried out on the Sparacia plots and ephemeral gully (EG) and gully measurements available in the literature, demonstrated that Equation (1) applies to rills, EGs, and gullies with b = 1.1 and a equal to 0.0036 for rills, 0.0984 for EGs, and 35.8 for gullies. Di Stefano et al. [27] confirmed the applicability of Equation (1) with b = 1.1 and the above scale factors using 475 (L–V) pairs detected on rills at Sparacia, EG measurements [26], and gully measurements conducted by Ichim et al. [28], Daba et al. [29], and Moges and Holden [30].

In accordance with Vandaele [31], Equation (1) establishes that the channelized erosion is a non-linear process in which the eroded volume rises more than proportionally with channel length. Therefore, the length of the channel can be regarded as an index of the severity of the erosion process.

This paper presents the results of an experimental investigation carried out at the Sparacia station. At first, for a rainfall erosive event (24 September 2017), terrestrial photogrammetric (TP) surveys of plots with different steepness incised by rills were carried out to reconstruct the Digital Surface Models (DSMs). The non-contributing network was distinguished from the contributing one using the method proposed by Carollo et al. [21], even if additional threshold values of L_T were investigated. The specific aims of this paper are to (i) establish the effect of plot steepness on rill depths and some morphometric characteristics of the drainage rill network (length and number of rills) and the corresponding index (i.e., drainage density and drainage frequency); (ii) test and calibrate Equation (1) using all rill measurements available in the literature [32] and those obtained in this study to establish whether only rill length is sufficient to estimate its volume; and (iii) modify Equation (1) by including climate forcing (event rainfall erosivity R_e) and assessing the related performance in the V estimation.

2. Materials and Methods

2.1. Study Area

The Sparacia experimental station of the Department of Agriculture, Food, and Forest Sciences of the University of Palermo is located in western Sicily, Southern Italy (37°38′09″N 13°45′58″E) (Figure 1). The area has a typical Mediterranean semiarid climate with an average annual rainfall of approximately 700 mm. The soil is a Vertic Haploxerept [33], and

the soil texture is constituted, on average, by 62% clay, 33% silt, and 5% sand, resulting in a clay soil [32].

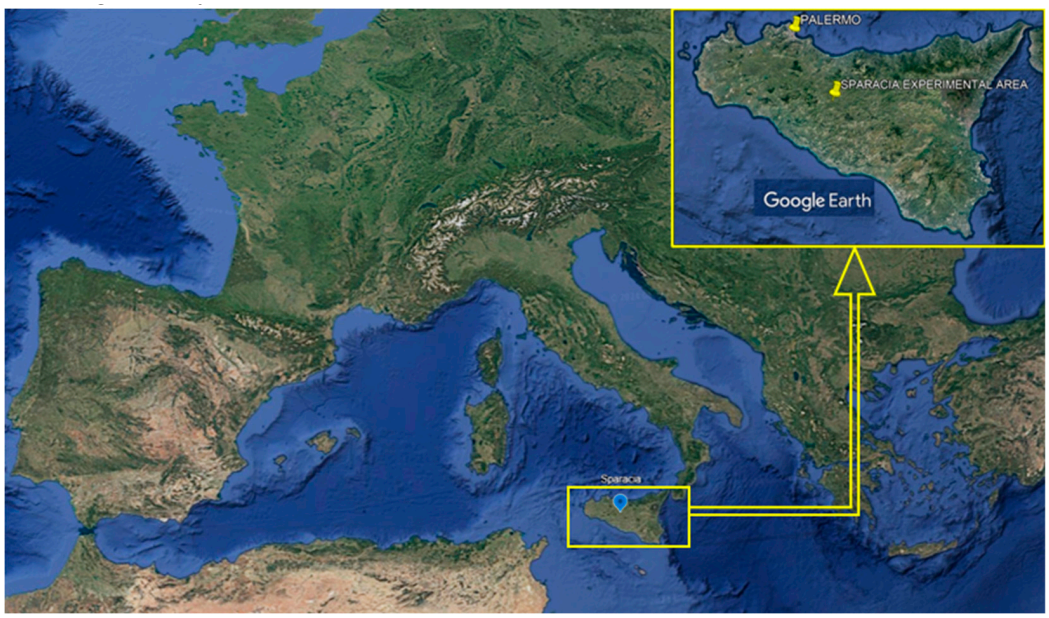

Figure 1. Location of Sparacia experimental area.

In this area, there are 20 USLE-type plots, having lengths from 11 to 44 m, widths from 2 to 8 m, and steepness s from 9% to 26%. In the 14.9% slope (Figure 2a), there are two plots (C–D) of 8 m × 18 m, two plots (E–F) of 8 m × 22 m, two plots (G–H) of 8 m × 33 m, two plots (I–L) of 8 m × 44 m, two plots (M–N) of 4 m × 11 m, two plots (O–P) of 2 m × 11 m, and two plots (Q–R) of 2 m × 22 m. In a near slope, there are two plots (P1–P2) of 6 m × 22 m (Figure 2b) characterized by s = 22% and two (P3–P4) plots of 6 m× 22 m (Figure 2b), which feature s = 26%. Finally, in the experimental area, there are two reference plots (W1–W2), which are 22 m long and 9% sloped (Figure 2c). All plots are in fallow condition, and the vegetation is removed by a powered cultivator operated in the maximum slope direction, as prescribed for the reference condition [34].

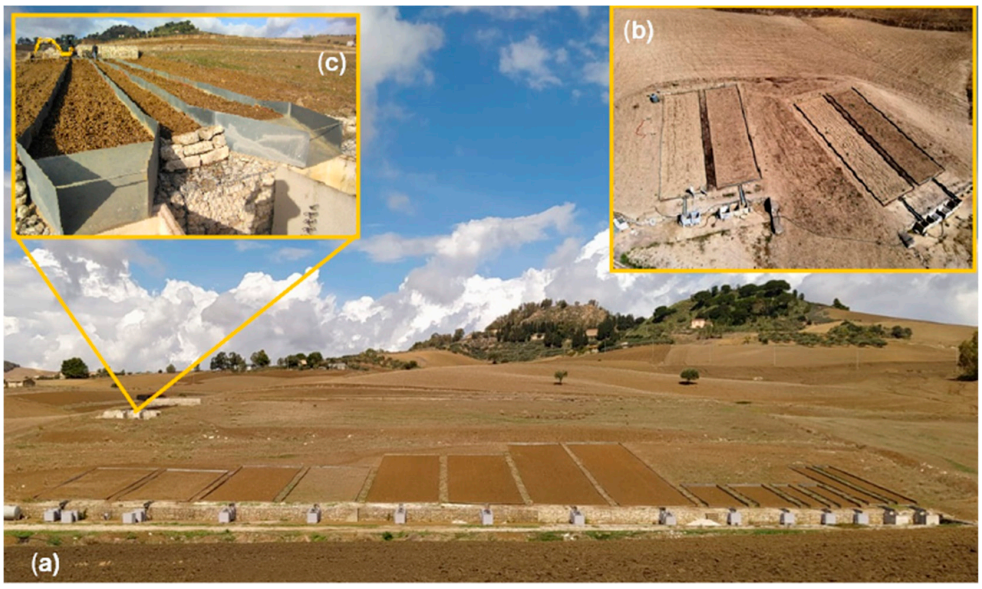

Figure 2. A view of the plots with slope gradient s equal to 0.149 (**a**), 0.22 and 0.26 (**b**), and 0.09 (**c**) at the Sparacia experimental area.

Runoff and transported soil particles are conveyed through a gutter located at the plot's lower edge towards a series of tanks, each one approximately 1 m^3 (Figure 3). Total soil loss and runoff are measured at event temporal scale. Rainfall intensity is measured with an acquisition interval of 1 min by a recording rain gauge placed near the plots.

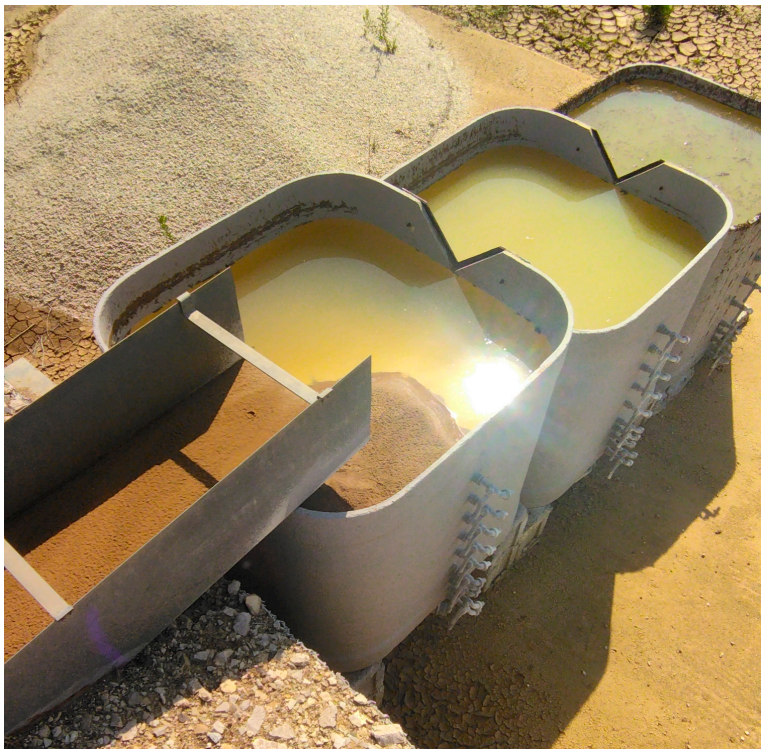

Figure 3. View of storage tanks.

2.2. Measurements of Total Soil Loss and Rill Erosion

For the severe erosive event of 24 September 2017, which was characterized by a total rainfall amount of 35.2 mm, total and rill erosion were measured for the P2, P4, and I plots (Figure 4). The total soil loss was measured by the direct method (DM) described below. For each tank, the level of the suspension of water plus sediments was measured and then thoroughly mixed before the extraction of five columns of suspension, extending across the entire suspension depth, with a sampler. It was a brass cylinder equipped with a closing valve "guillotine" fitted with a sealing gasket. Further details are reported in the paper by Carollo et al. [35]. The sample was oven-dried at 105 °C for 48 h, and the dry sediment was weighed. The suspension concentration was determined as dry sediment weight to suspension volume ratio, the latter being determined gravimetrically. Following Carollo et al. [35], the measured and the actual concentration could be considered coincident, and the margin of measurement error declined for increasing values of the actual concentration. Total soil loss was determined by multiplying the sediment concentration by suspension volume.

The rill measurements were performed by a terrestrial photographic survey (TP). The 12 MP GoPro Hero4 Silver camera [36] was fixed to the tip of a telescopic pole (Figure 5a) for image acquisition by following a walking itinerary around the plots. The average object distance H was equal to 2.4 m, and 325, 140, and 140 images were taken for plots I, P2, and P4, respectively. Six Ground Control points (GCPs) per plot, made of 15 cm × 15 cm wooden targets (Figure 5b), were deployed on the perimeter, and the coordinates were determined using a total topographic station.

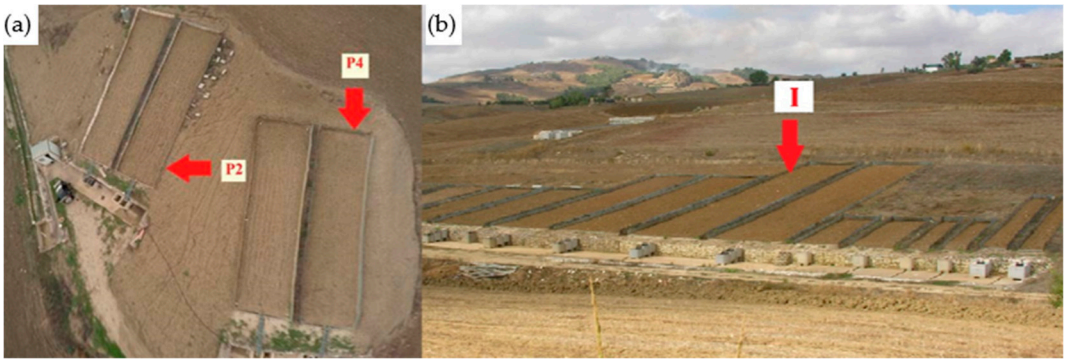

Figure 4. View of investigated plots P2 and P4 (**a**) and I (**b**).

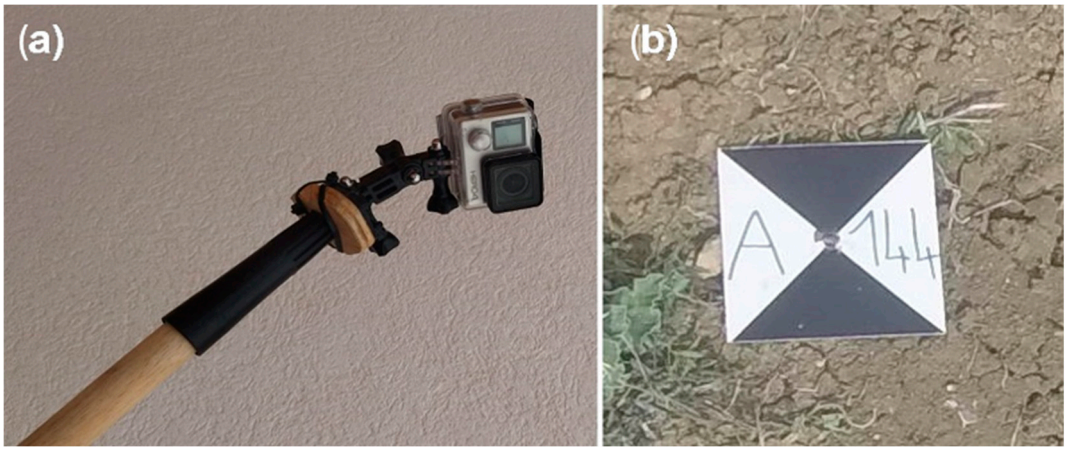

Figure 5. A view of the GoPro camera (**a**) and the target of a GCP (**b**).

The software Agisoft PhotoScan Professional Edition 1.1.6 build2038 (Agisoft LLC, Petersburg, Russia) allowed the creation of 3D models and, later, 2.5D models (Digital Surface Models, DSMs) and orthophotos of the investigated plots by using photographs as raw data. The 3D models were created using an automated procedure combining Multi-view stereo [37] and Structure from Motion (SfM) techniques [13]. For each plot, a DSM (Figure 6a) and an orthophoto (Figure 6b) were generated by Agisoft Photoscan to perform hydrological and morphological analyses aimed to extract the rill network. The mean ground sample distance, GSD, which is the size of a pixel projected to the ground surface expressed as linear units [20], is 0.0015 m, while the DEM resolution (0.005 m) corresponds to the better achievable resolution suggested by PhotoScan considering the GSD values. As mentioned above, to extract rill thalweg from the DSMs, a method that combines morphological (convergence index *CI*) and hydrological (flow accumulation ArcGIS's 10.5 tool, (ESRI, Redlands, CA, USA)) analyses was applied [20,21,38]. The convergence index is expressed as follows:

$$CI = \left(\frac{1}{n-1} \sum_{i=1}^{n-1} \theta_i \right) - 90 \quad (2)$$

where n is the number of kernel cells, and for each external cell i, θ_i is the angle, in degrees, between the aspect of cell i and the direction of the vector joining the center of cell i and the center of the kernel. A *CI* threshold, equal to the mean minus two times the standard deviation of *CI*, was determined to identify the cells constituting the channel [18–20]. The disconnected convergent areas were identified and considered as rill features. To connect these rill features and delineate the GRID of the thalweg, the flow accumulation algorithm was weighted with the GRID of the convergence index.

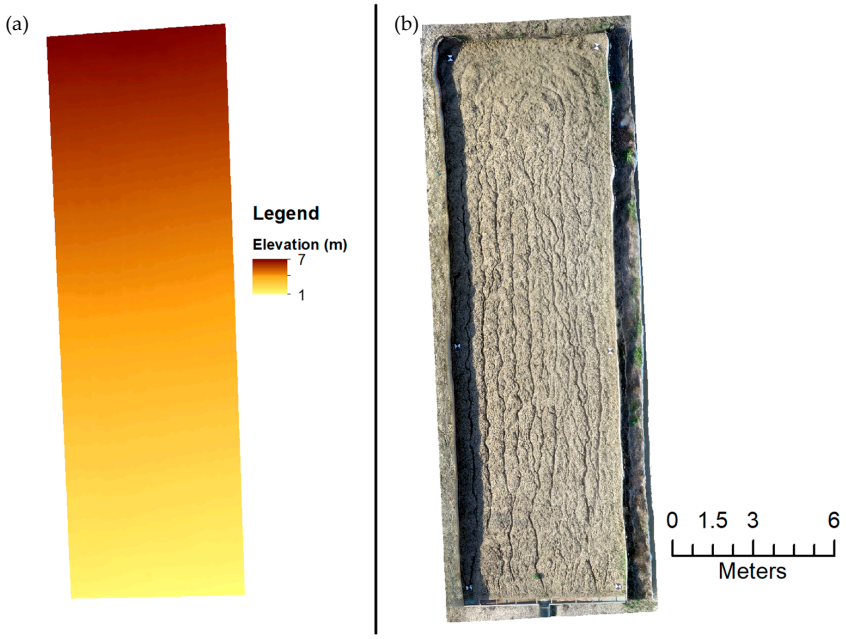

Figure 6. Digital Surface Model (DSM) (**a**) and orthophoto (**b**) obtained for plot P4.

Due to sediment delivery processes in rilled areas [23,27,32], only a part of the eroded particles reaches the plot outlet, and some rills are interrupted within the plot. For considering these processes, here, rills were separated into contributing and non-contributing rills. To select the former, the automatic procedure proposed by Di Stefano et al. [20] was applied. First, the focal statistics tool (*Focal_max*) of ArcGIS was applied to the DSM for performing a neighborhood operation that computed an output raster where the cell value was the maximum of all the input cells' values falling in a neighborhood around that location. The neighborhood was a rectangle 30 cm wide and 1 cell high. Then, the *Focal_max* and DSM were subtracted to create a raster of deepening, h_d, referring to the maximum elevation in the pixel neighborhood. Rill interruptions were identified where the condition of h_d under a threshold, h_T, persisted for at least more than a rill length threshold L_T. In this case, the upstream rill reach was classified as non-contributing. In this investigation, a single h_T of 1 cm and different L_T values were used. In particular, to determine the L_T value that minimizes the error in soil loss measurement, for plot I, two L_T values of 18 and 20 cm were used, in addition to 10, 12, and 15 cm used in a previous investigation [21]. For plots P2 and P4, only L_T = 10 cm was tested as explained below. To measure the rill volume V, each channel was divided into segments, each of them bounded by two 0.3 m wide transects perpendicular to the thalweg and with distance d equal to 0.3 m. The cross-section profiles were extracted at the transects from the point cloud of the 3D model by Cloud Compare v2.10.2 software (www.cloudcompare.org). The depth, h, and the cross-section area, σ, were measured by AutoCad 2015 (Autodesk, San Francisco, CA, USA), and the volume $V_{r,s}$ of the rill segment was calculated via Equation (3):

$$V_{r,s} = 0.5(\sigma_i + \sigma_{i+1})d \quad (3)$$

where σ_i and σ_{i+1} are the cross-section areas bounding the rill segment. The sum of $V_{r,s}$ gives the total volume V, which was converted into weight by the mean value of bulk density, equal to 1200 kg m^{-3}. The soil loss measured by DM, A, was the reference to evaluate the error E (%) for the TP measurement, A_{LT}, deriving from the use of different L_T values:

$$E = \left(\frac{A_{LT} - A}{A}\right)100 \quad (4)$$

To compare the rill networks of the three investigated plots, some morphometric indexes were determined. Specifically, the drainage density D_k and the drainage frequency F_k were calculated as follows:

$$D_k = \frac{LR}{AR} \quad (5)$$

$$F_k = \frac{N}{AR} \quad (6)$$

where LR is the total length of the rill network, N is the number of detected rills, and AR is the plot area. The drainage frequency is an indicator of network complexity, while the drainage density indicates the network extent and how effectively it delivers sediment.

2.3. Modeling Rill Erosion

In the period November 2004–September 2017, the rill survey in the Sparacia experimental area was conducted for eleven events. For each event, Table 1 lists the monitored plots, the total rainfall P_e (mm), the event rainfall erosivity index R_e (MJ mm ha^{-1} h^{-1}), and N. R_e [34] is the product of the maximum rainfall intensity with a duration of 30 min and rainfall kinetic energy per unit area.

Table 1. Characteristic data of the erosive events: monitored plots, rainfall amount, P_e (mm), event rainfall erosivity index, R_e (MJ mm ha^{-1} h^{-1}), number of detected rills N, and total number of rills N_T.

Event	Plot	P_e	R_e	N
5 November 2004	P1	49.4	122.2	10
16 November 2004	P1	53.8	341.6	13
13 December 2005	P1	97.8	334.0	8
1 September 2005	C-P1-G	64.6	975.9	50
28 June 2008	P2/A-C-D-E-G-H-I-L	52.2	680.1	144
1 October 2008	P2-P1/A-C-D-G-H-I-L-M-N-P	30.6	154.4	157
1 November 2008	P3-P4	15.8	96.5	20
18 October 2008	E	116.2	393.8	19
3 October 2011	C	28.0	402.0	23
24 October 2016	P2/P3	18.8	102.3	79
24 September 2017	P2/P3-P4/I	35.2	571.1	208
			N_T	731

Using all the available rill measurements (731 L–V pairs), Equation (1) with a = 0.0036 and b = 1.1 determined by Di Stefano and Ferro [26], Equation (1) with recalibrated values of the a and b coefficients, and a rearranged version of this model, which includes the event rainfall erosivity index, were tested. The model performances were evaluated by the comparison between the measured, $V_{measured}$, and estimated, $V_{calculated}$, rill volumes and the root-mean-square error, $RMSE$:

$$RMSE = \sqrt{\frac{\sum_{i=1}^{N_T}(V_{measured} - V_{calculated})_i^2}{N_T}} \quad (7)$$

where N_T is the total number of investigated rills (Table 1).

3. Results

3.1. Automatic Extraction of Contributing Rill Network to Plot Soil Loss

For the I plot, Figure 7a shows that, as expected, the weight of soil loss A (kg) increases as L_T increases. These measurements were affected by errors shown in Figure 7b, which points out that L_T = 18 cm is the threshold value that minimizes the error (E = −13%).

For plots P2 and P4, the single L_T minimum value, equal to 10 cm, was applied because it led to identifying a limited number of rill interruptions and almost the entire rill network as contributing. Therefore, L_T values higher than 10 cm would not have produced changes

in terms of the contributing network. Figure 8a shows that, for both plots, the soil loss measurements carried out by the TP method are comparable with those obtained by DM. In particular, they are affected by errors equal to −4% and +10% for P2 and P4 plots, respectively. Figure 8b shows that both for TP and DM, soil loss per unit area (kg m^{-2}) increases with plot steepness and confirms the validity of the assumptions made to detect the contributing rill network and the reliability of the SfM technique to measure rill erosion for all three plots ($-13\% \leq E \leq +10\%$).

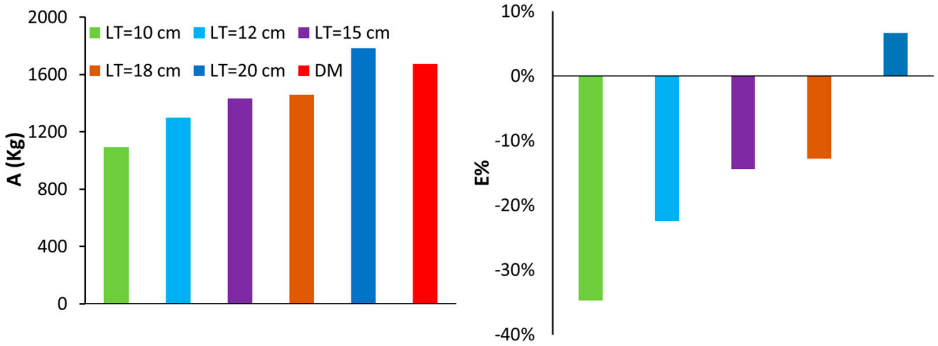

(**a**) (**b**)

Figure 7. Comparison of soil loss A measured in plot I by using different threshold values L_T that identify rill interruption length and DM (**a**), and corresponding error values (**b**).

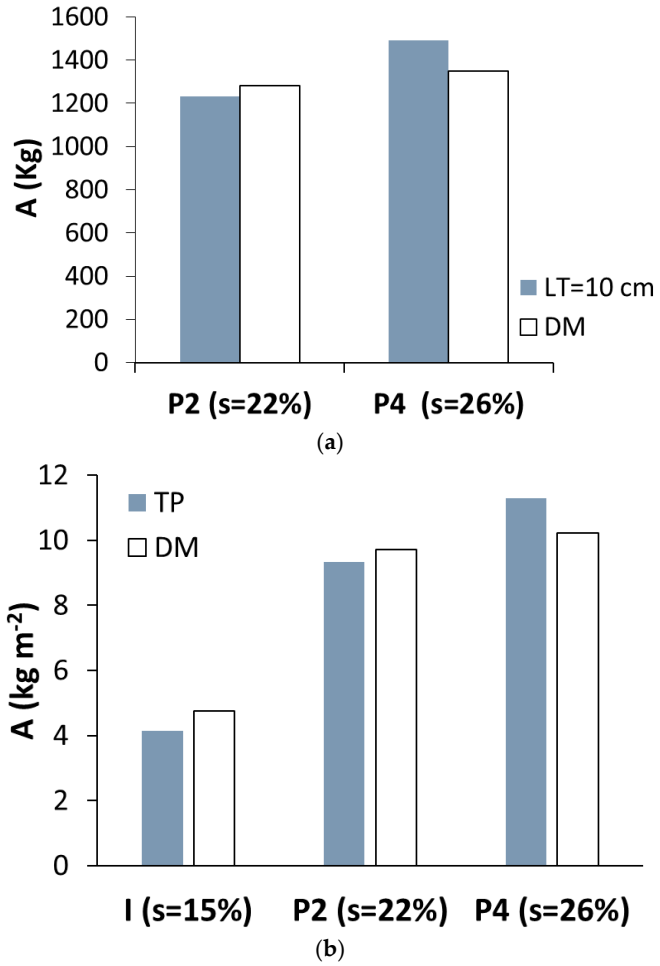

(**a**)

(**b**)

Figure 8. Comparison between soil loss A measured in plots P2 and P4 by using a threshold value L_T = 10 cm and DM (**a**), and relation between plot steepness and soil loss per unit area measured with the indirect method and DM (**b**).

The rill depths and some morphometric indexes of the rill networks surveyed in the three plots were also compared. The cumulative frequency distributions of rill depth F(h) plotted in Figure 9 show that h increases as plot steepness increases.

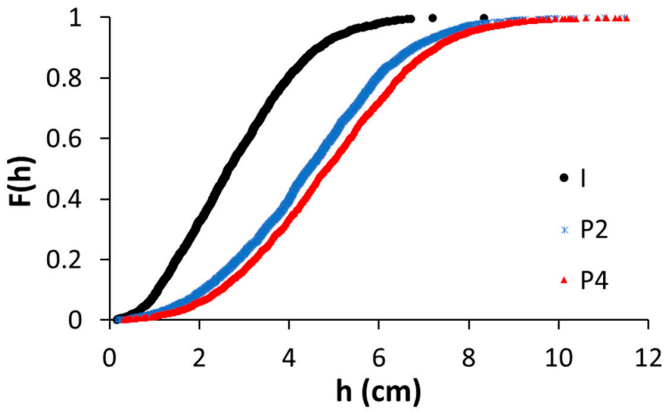

Figure 9. Cumulative frequency distributions of rill depth h.

Figure 10 shows the values of drainage density (Figure 10a) and frequency (Figure 10b) for non-contributing, contributing, and total rill network surveyed in the three plots. For the I and P2 plots, the D_k and F_k values of the total rill network are comparable, whereas they are higher for P4. The length of contributing rills on the I plot is about 50% of the total length, while for the P2 and P4 plots the length of non-contributing rills is negligible, representing only 4 and 7% of the total length, respectively. Finally, for the I plot, 63% of the rills did not contribute to soil loss, while in the two steeper plots the number of non-contributing rills was limited (<10%).

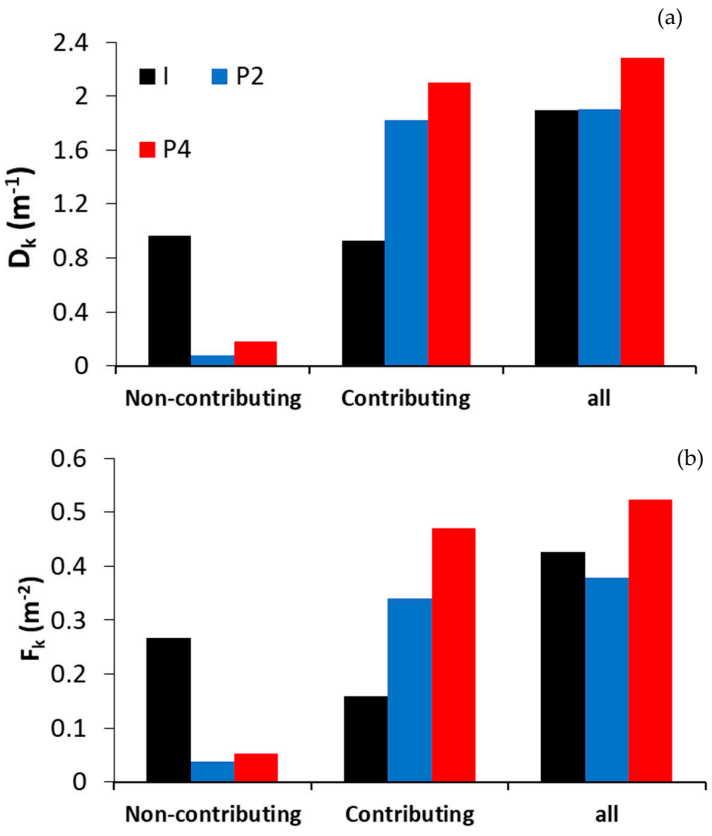

Figure 10. Values of drainage density D_k (**a**) and frequency F_k (**b**) distinguished for non-contributing, contributing, and total rill networks.

3.2. Relationship Between Rill Length and Eroded Volume

At first, the data collected for the rainfall erosive events of this investigation and those available in the literature [20,27] were used to test the equation for estimating the total eroded volume V (Equation (1)) proposed by Nachtergaele et al. [24], using the coefficients a = 0.0036 and b = 1.1 determined by Di Stefano and Ferro [26]. Figure 11 shows the comparison between the measured V values and those calculated by Equation (1) with a = 0.0036 and b = 1.1.

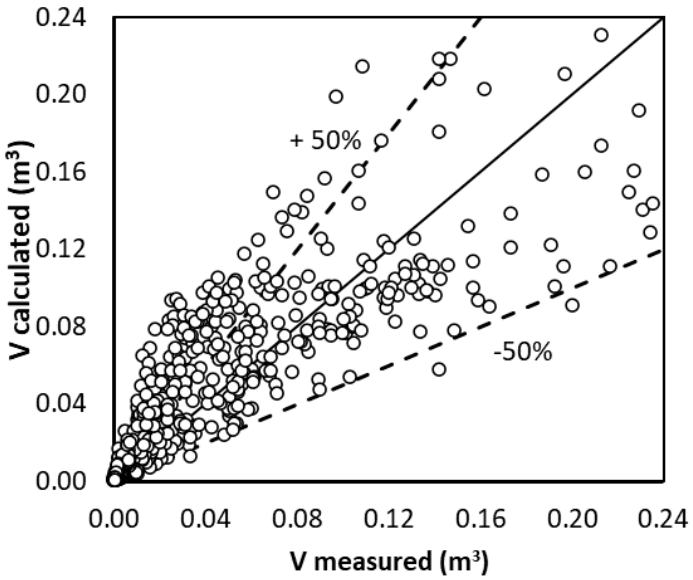

Figure 11. Comparison between the measured total eroded volume V values and those calculated by Equation (1) with a = 0.0036 and b = 1.1.

In this case, the errors $E_V = (V_{calculated} - V_{measured})/V_{measured}$ in the V estimate are within the error bands of ±75% for 66% of cases and ±50% for 56% of cases, with an $RMSE$ of 0.0276. This result suggests the need to recalibrate the V–L relationship developed in the literature for rills (Equation (1) with a = 0.0036 and b = 1.1). Considering all the new available measurements, Equation (1) was recalibrated (Figure 12a), obtaining a = 0.0024 and b = 1.167. The comparison between the measured volumes and those obtained by the recalibrated relationship (Figure 12b) yields errors E_V that are within the error bands of ±75% for 81% of cases and ±50% for 63% of cases and an $RMSE$ of 0.0287.

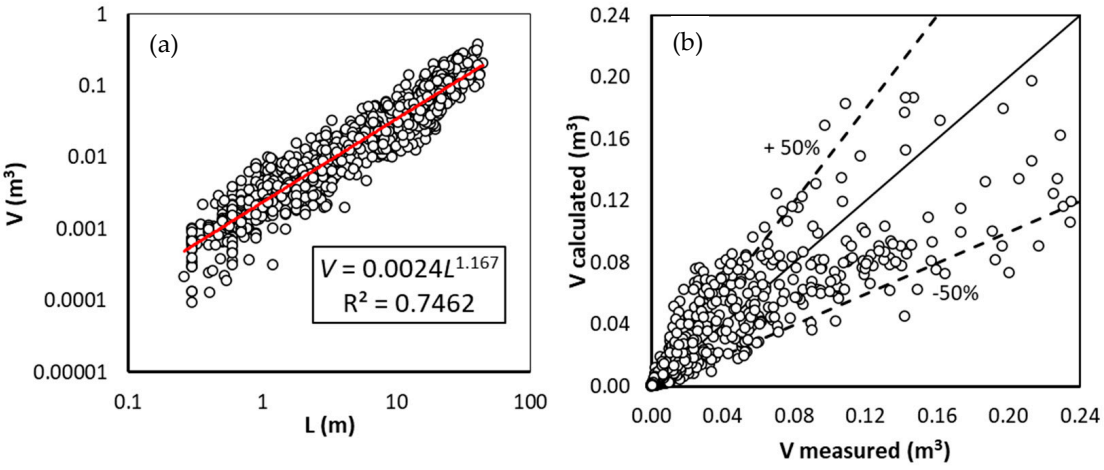

Figure 12. The relationship between the measured eroded volumes V and rill length L values (**a**) and the comparison between the measured V values and those calculated by Equation (1) with a = 0.0024 and b = 1.167 (**b**).

This not-satisfying result suggested considering another variable characterizing the erosive event. For this reason, Equation (1) was recalibrated, distinguishing the data of each erosive event. Figure 13 shows the values of the a (Figure 13a) and b (Figure 13b) coefficients obtained for the investigated rainfall events, characterized by the statistics reported in Table 2. This figure and the data reported in Table 2 highlight that the a coefficient varies in a large range, while the b coefficient, except for two data points, is characterized by a limited variability. Therefore, Equation (1) was calibrated, fixing the weighted arithmetic mean of the b coefficient (1.3), in which the weights are the ratios of the number of rills per event to N_T, and attributing all the variability to the a coefficient.

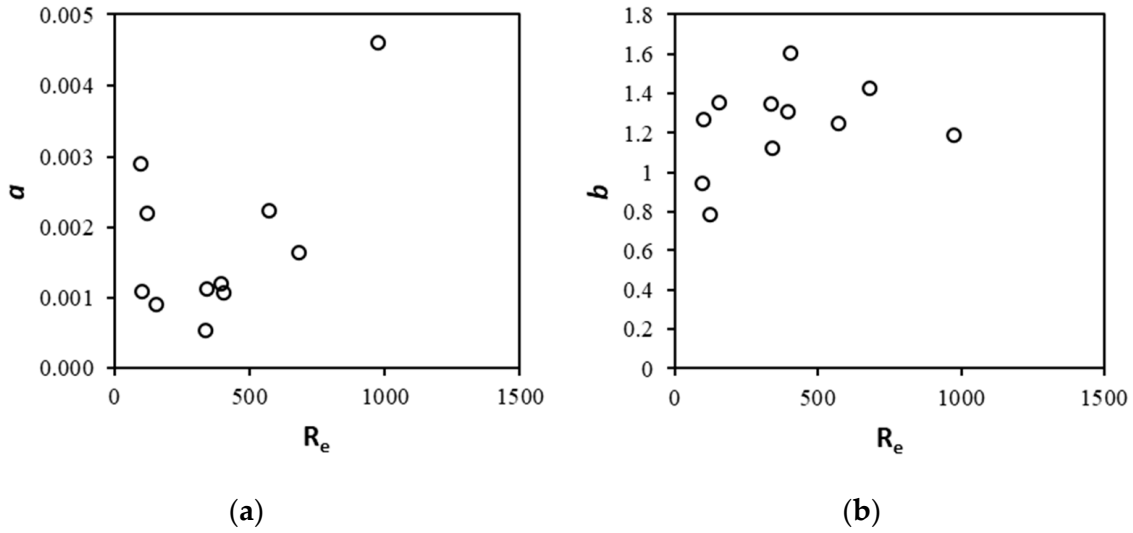

(**a**) (**b**)

Figure 13. The relationship between the rainfall event erosivity index R_e and the a (**a**) and b (**b**) coefficients of Equation (1).

Table 2. Statistics of a and b coefficients obtained by calibrating Equation (1) for each erosive event.

	a	b	a with b = 1.3
Mean	0.00173	1.24	0.0016
Standard deviation	0.00123	0.23	0.0009
Coefficient of variation (CV)	0.71037	0.18	0.57
Min	0.00054	0.79	0.0006
Max	0.00461	1.61	0.0033
Weighted arithmetic mean		1.3	

To assess if the a coefficient is related to the rainfall characteristics, the relationship between the a values obtained with b = 1.3 and R_e was investigated (Figure 14a). This figure underlines that a linear relationship exists between these two variables, confirming that the rainfall characteristics of the erosive event play a significant role in the rill scouring processes. Equation (1) can be rewritten as follows:

$$V = 4 \times 10^{-6} R_e L^{1.3} \quad (8)$$

Equation (8) is characterized by E_V lower than or equal to 75% for 87% of cases and lower than or equal to 50% for 65% of cases (Figure 14b) and an RMSE of 0.0182, which highlights that considering the rainfall event erosivity allows for improving the estimate of the rill eroded volume.

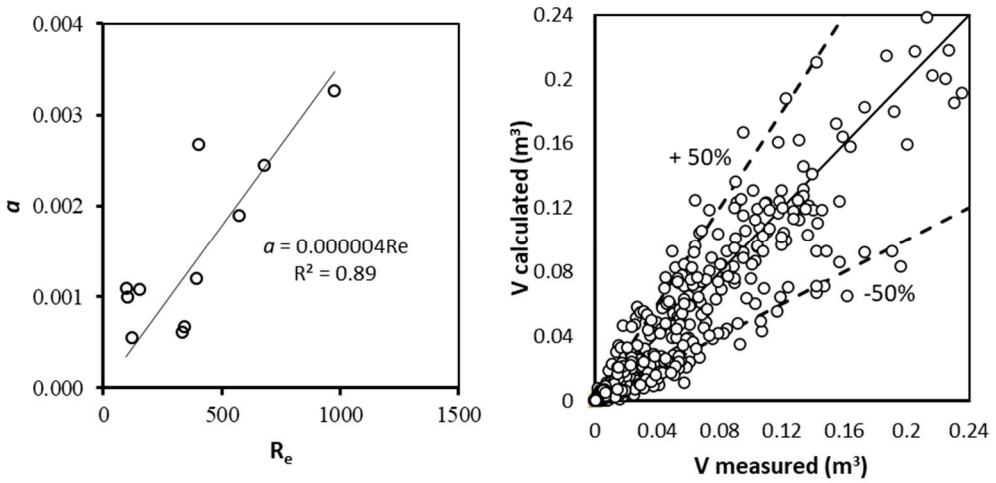

(**a**) (**b**)

Figure 14. The relationship between the a values obtained with b = 1.3 and the rainfall event erosivity R_e (**a**) and the comparison between the measured total eroded volume V values and those calculated by Equation (8) (**b**).

Moreover, considering that R_e is a significant variable influencing the investigated relationship, the multiple regression analysis was performed to evaluate if a further improvement in the performances of the V estimate can be pursued. This analysis led to the following equation:

$$V = 1.61 \times 10^{-4} R_e^{0.465} L^{1.144} \quad (9)$$

which yields the results plotted in Figure 15. In detail, Equation (9) gives E_V within the error bands of ±75% for 89% of cases and ±50% for 78% of cases, with an RMSE of 0.0187. Figure 16 shows the frequency distribution of the errors obtained by the tested approaches.

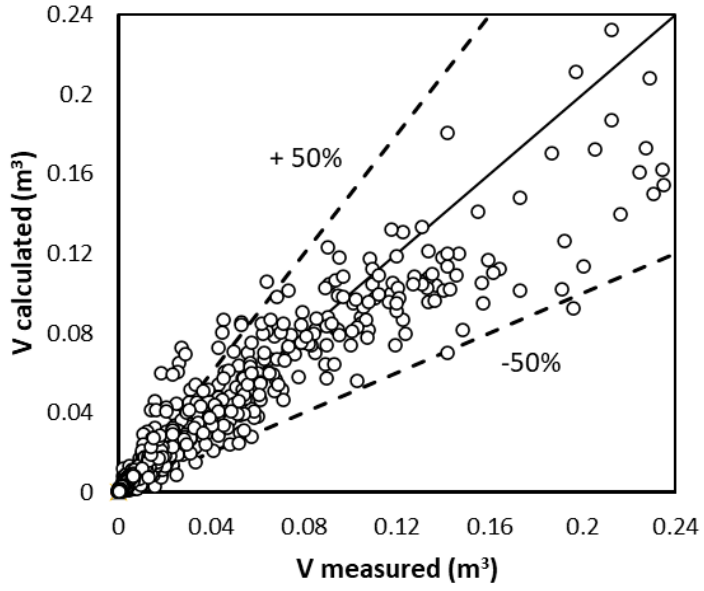

Figure 15. A comparison between the measured total eroded volume V values and those calculated by Equation (9).

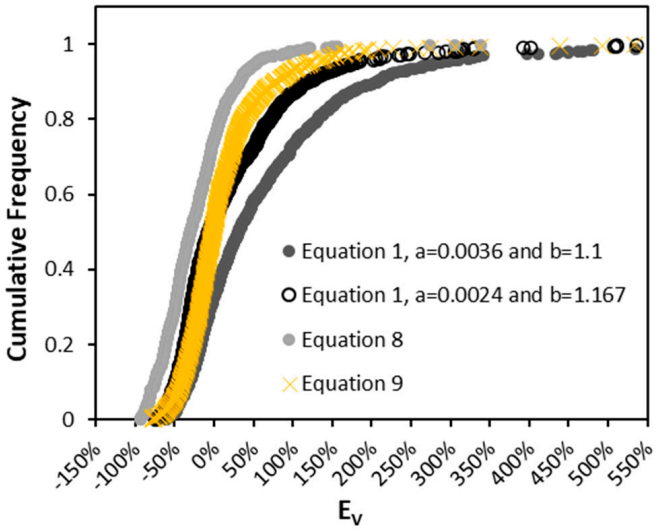

Figure 16. An empirical frequency distribution of the errors E_V in the volume estimate obtained for each of the tested models.

4. Discussion

4.1. Automatic Extraction of Contributing Rill Network to Plot Soil Loss

The result obtained for plot I (Figure 7a) is due to the fact that as L_T increases, the number of interruptions decreases and therefore the length of the contributing network increases. The general soil loss underestimation (Figure 7) can be explained by the fact that DM also includes the contribution of the inter-rill component, even if it is the minor erosion component, while TP considers only the rill component, which is roughly 80% of the total erosion [1,6]. For the same reason, the overestimation for L_T = 20 cm is unrealistic. Therefore, even though L_T = 20 cm is associated with the minimum absolute error, as it gives a positive error, the corresponding soil loss measurement was considered less accurate than that obtained with L_T = 18 cm. Instead, the results obtained for the plots P2 and P4 (s = 22 and 26%) (Figure 8) highlighted that the L_T values higher than 10 cm cannot be applied, as the threshold of 10 cm identifies the entire rill network as contributing. These results, combined with those obtained by Carollo et al. [21], who found an optimal L_T value (i.e., the lowest negative errors in soil loss estimate) equal to 15 cm, underline that the threshold value is sensitive to the investigated data. Figure 9 underlines that steepness affects the erosion phenomena and deepening processes of the rill network. This result agrees with the conclusions reported by Carollo et al. [21] and confirms that steep slopes (s > 18%) are characterized by more intense erosive phenomena than gentle ones [39,40]. Figure 10 suggests that, for the present erosive event, the planimetric development of the total rill network is weakly affected by plot steepness, while the length and the number of contributing rills increase with increasing plot steepness. In other words, the rill network becomes more efficient and contributes more to the flow and sediment transport in steeper slopes. The found increasing relationship between drainage density and plot steepness detected for the contributing rills agrees with the findings available in the literature [20,41–43].

4.2. Relationship Between Rill Length and Eroded Volume

The comparison between the results (Figure 11) obtained by applying Equation (1) with the a (0.0036) and b (1.1) coefficients available in the literature [26] and those (Figure 12b) obtained with the recalibrated Equation (1) (a = 0.0024 and b = 1.167) highlights that, even if the *RMSE* values are comparable, the second one leads to a better performance in terms of E_V. The developed analysis shows that the inclusion of the rainfall event erosivity R_e into the model significantly improves its reliability, as demonstrated by the E_V and *RMSE* values. In detail, even if the *RMSE* values obtained for Equations (8) and (9) are comparable, Figures 14b, 15 and 16 point out that Equation (8) tends to underestimate the

eroded volumes, while Equation (9) has the best balance between underestimation and overestimation, leading to the best performance in the V estimate. In conclusion, the results of this investigation demonstrated that including the event rainfall erosivity in the model allows for accounting for a significant variable driving the channelized erosive phenomena. This last information can be very useful for future studies investigating eroded volumes in erosive forms, such as rills, on hillslopes. In fact, a model considering the impact of climate forcing allows for estimating the geometrical features of the rill channel occurring for an erosive event with specific rainfall characteristics. In other words, the rill channel print can be modeled at the event temporal scale. The main limitation of this paper is that the measurements were collected only for a single experimental area, having a unique soil texture, and a restricted range of R_e characterizing the rainfall events, and thus these results have to be tested for other geographical areas, characterized by different soils and rainfall characteristics.

5. Conclusions

In this investigation, for the severe erosive event that occurred in September 2017 at the Sparacia experimental area, three experimental plots with different length and steepness values incised by rills were surveyed by terrestrial photogrammetry to reconstruct the DSMs. For each plot, the rill network was extracted from the DSMs, and the non-contributing network was distinguished from the contributing one. The eroded volumes V, from which the soil loss was computed, were determined on the latter. The analysis demonstrated that h, drainage density, and drainage frequency of the contributing rill network increase with plot steepness. In particular, the mean depth increases from 2.79 to 4.85 cm for slope increasing from 14.9 to 26%. Moreover, the drainage frequency of the contributing rill network varies from 0.16 m^{-2} for s = 14.9% to 0.47 m^{-2} for s = 26%, while the drainage density of the contributing rill network varies from 0.92 m^{-1} for s = 14.9% to 2.1 m^{-1} for s = 26%. Finally, using the data available in the literature and those obtained in this investigation, an empirical relationship between V and the total rill length L was first assessed and then rearranged considering the rainfall erosivity R_e. Including R_e, and thus considering the climate forcing, in the rearranged equation guaranteed the best performance (E_V within the error bands of $\pm$75% for 89% of cases and $\pm$50% for 78% of cases, with an RMSE of 0.0187) in volume estimation.

Author Contributions: Conceptualization, V.P. (Vincenzo Palmeri), C.D.S., A.N., V.P. (Vincenzo Pampalone), and V.F.; methodology, V.P. (Vincenzo Palmeri), C.D.S., A.N., V.P. (Vincenzo Pampalone), and V.F.; software, V.P. (Vincenzo Palmeri), C.D.S., A.N., V.P. (Vincenzo Pampalone), and V.F.; validation, V.P. (Vincenzo Palmeri), C.D.S., A.N., V.P. (Vincenzo Pampalone), and V.F.; formal analysis, V.P. (Vincenzo Palmeri), C.D.S., A.N., V.P. (Vincenzo Pampalone), and V.F.; investigation, V.P. (Vincenzo Palmeri), C.D.S., A.N., V.P. (Vincenzo Pampalone), and V.F.; data curation, V.P. (Vincenzo Palmeri), C.D.S., A.N., V.P. (Vincenzo Pampalone), and V.F.; writing—original draft preparation, V.P. (Vincenzo Palmeri), C.D.S., A.N., V.P. (Vincenzo Pampalone), and V.F.; writing—review and editing, V.P. (Vincenzo Palmeri), C.D.S., A.N., V.P. (Vincenzo Pampalone), and V.F.; visualization, V.P. (Vincenzo Palmeri), C.D.S., A.N., V.P. (Vincenzo Pampalone), and V.F.; supervision, C.D.S. and V.F.; project administration, V.P. (Vincenzo Pampalone) and V.F.; funding acquisition, V.P. (Vincenzo Pampalone) and V.F. All authors have read and agreed to the published version of the manuscript.

Funding: This study was carried out within the PRIN project "Soil Conservation for sustainable AgricuLture in the framework of the European green deal" (SCALE) and received funding from the European Union—NextGenerationEU Project (National Recovery and Resilience Plan—NRPP, M4.C2.1.1., project 2022PB2NSP_002, CUP B53D23017980006). The project was also developed under the National Recovery and Resilience Plan (NRRP), Mission 4, Component 2, Investment 1.4—Call for tender no. 3138 of 16 December 2021, rectified by Decree no. 3175 of 18 December 2021 of the Italian Ministry of University and Research funded by the European Union—NextGenerationEU Project Code CN_00000033, Concession Decree no. 1034 of 17 June 2022 adopted by the Italian Ministry of University and Research, CUP B73C22000790001, Project Title "National Biodiversity Future Center (NBFC)".

Data Availability Statement: The datasets analyzed during the current study are not publicly available but are available from the corresponding author on reasonable request.

Conflicts of Interest: The authors declare no conflicts of interest.

References

1. Di Stefano, C.; Nicosia, A.; Palmeri, V.; Pampalone, V.; Ferro, V. Rill flow velocity and resistance law: A review. *Earth-Sci. Rev.* **2022**, *231*, 104092. [CrossRef]
2. Shi, H.; Xiao, H.; Liu, G.; Abd Elbasit, M.A.; Zheng, F.; Zhang, Q.; Zhang, Y.; Guo, Z. Identifying interrill, rill, and ephemeral gully erosion evolution by using rare earth elements as tracers. *J. Hydrol.* **2022**, *612*, 128271. [CrossRef]
3. Luo, J.; Zheng, Z.; Li, T.; He, S.; Zhang, X.; Huang, H.; Wang, Y. Quantifying the contributions of soil surface microtopography and sediment concentration to rill erosion. *Sci. Total Environ.* **2021**, *752*, 141886. [CrossRef] [PubMed]
4. Foster, G.R.; Huggins, L.F.; Meyer, L.D. A laboratory study of rill hydraulics: I. Velocity relationships. *Trans. ASAE* **1984**, *27*, 790–796. [CrossRef]
5. Carollo, F.G.; Di Stefano, C.; Nicosia, A.; Palmeri, V.; Pampalone, V.; Ferro, V. Flow resistance in mobile bed rills shaped in soils with different texture. *Eur. J. Soil Sci.* **2021**, *72*, 2062–2075. [CrossRef]
6. Mutchler, C.K.; Young, R.A. Soil detachment by raindrops. In *Present and Prospective Technology for Predicting Sediment Yields and Sources*; ARS-S-40; Agricultural Research Service: Washington, DC, USA, 1975; pp. 113–117.
7. Di Stefano, C.; Nicosia, A.; Palmeri, V.; Pampalone, V.; Ferro, V. Rill flow resistance law under sediment transport. *J. Soils Sediments* **2022**, *22*, 334–347. [CrossRef]
8. Liu, G.; Zheng, F.; Wilson, G.V.; Xu, X.; Liu, C. Three decades of ephemeral gully erosion studies. *Soil. Tillage Res.* **2021**, *212*, 105046. [CrossRef]
9. Wang, N.; Luo, J.; He, S.; Li, T.; Zhao, Y.; Zhang, X.; Wang, Y.; Huang, H.; Yu, H.; Ye, D.; et al. Characterizing the rill erosion process from eroded morphology and sediment connectivity on purple soil slope with upslope earthen dike terraces. *Sci. Total Environ.* **2023**, *860*, 160486. [CrossRef]
10. Eltner, A.; Baumgart, P.; Maas, H.G.; Faust, D. Multi-temporal UAV data for automatic measurement of rill and interrill erosion on loess soil. *Earth Surf. Process. Landf.* **2015**, *40*, 741–755. [CrossRef]
11. Vinci, A.; Brigante, R.; Todisco, F.; Mannocchi, F.; Radicioni, F. Measuring rill erosion by laser scanning. *Catena* **2015**, *124*, 97–108. [CrossRef]
12. Gessesse, G.; Fuchs, H.; Mansberger, R.; Klik, A.; Rieke-Zapp, D.H. Assessment of erosion, deposition and rill development on irregular soil surfaces using close range digital photogrammetry. *Photogramm. Rec.* **2010**, *25*, 299–318. [CrossRef]
13. Di Stefano, C.; Ferro, V.; Palmeri, V.; Pampalone, V. Measuring rill erosion using structure from motion: A plot experiment. *Catena* **2017**, *156*, 383–392. [CrossRef]
14. Jiang, Y.; Shi, H.; Wen, Z.; Guo, M.; Zhao, J.; Cao, X.; Fan, Y.; Zheng, C. The dynamic process of slope rill erosion analyzed with a digital close range photogrammetry observation system under laboratory conditions. *Geomorphology* **2020**, *350*, 106893. [CrossRef]
15. Jiang, Y.; Shi, H.; Wen, Z.; Guo, M.; Zhao, J.; Cao, X.; Shui, J.; Paull, D. A comparative experimental study of rill erosion on loess soil and clay loam soil based on a digital close-range photogrammetry technology. *Geomorphology* **2022**, *419*, 108487. [CrossRef]
16. Canny, J. A computational approach to edge detection. *IEEE Trans. Pattern Anal. Mach. Intell.* **1986**, *8*, 679–698. [CrossRef]
17. Broscoe, A.J. Quantitative analysis of longitudinal stream profiles of small watersheds. In *Technical Report*; New York Department of Geology, Columbia University: New York, NY, USA, 1959.
18. Pirotti, F.; Tarolli, P. Suitability of LiDAR point density and derived landform curvature maps for channel network extraction. *Hydrol. Process.* **2010**, *24*, 1187–1197. [CrossRef]
19. Tarolli, P.; Sofia, G.; Dalla Fontana, G. Geomorphic features extraction from high-resolution topography: Landslide crowns and bank erosion. *Nat. Hazards* **2012**, *61*, 65–83. [CrossRef]
20. Di Stefano, C.; Palmeri, V.; Pampalone, V. An automatic approach for rill network extraction to measure rill erosion by terrestrial and low-cost unmanned aerial vehicle photogrammetry. *Hydrol. Process.* **2019**, *33*, 1883–1895. [CrossRef]
21. Carollo, F.G.; Di Stefano, C.; Nicosia, A.; Palmeri, V.; Pampalone, V.; Ferro, V. Testing an automatic approach for rill network extraction to measure rill erosion by terrestrial photogrammetry. In Proceedings of the Conference of the Italian Society of Agricultural Engineering, Palermo, Italy, 19–22 September 2022; Springer: Berlin/Heidelberg, Germany, 2023; pp. 89–96.
22. Bruno, C.; Di Stefano, C.; Ferro, V. Field investigation on rilling in the experimental Sparacia area, South Italy. *Earth Surf. Proc. Land.* **2008**, *33*, 263–279. [CrossRef]
23. Rejman, J.; Brodowski, R. Rill characteristics and sediment transport as a function of slope length during a storm event on loess soil. *Earth Surface Processes and Landforms: J. Br. Geomorphol. Res. Group* **2005**, *30*, 231–239. [CrossRef]
24. Nachtergaele, J.; Poesen, J.; Steegen, A.; Takken, I.; Beuselinck, L.; Vandekerckhove, L.; Govers, G. The value of a physically based model versus an empirical approach in the prediction of ephemeral gully erosion for loess-derived soils. *Geomorphology* **2001**, *40*, 237–252. [CrossRef]
25. Capra, A.; Di Stefano, C.; Ferro, V.; Scicolone, B. Similarity between morphological characteristics of rills and ephemeral gullies in Sicily, Italy. *Hydrol. Process.* **2009**, *23*, 3334–3341. [CrossRef]
26. Di Stefano, C.; Ferro, V. Measurements of rill and gully erosion in Sicily. *Hydrol. Process.* **2011**, *25*, 2221–2227. [CrossRef]

27. Di Stefano, C.; Ferro, V.; Pampalone, V.; Sanzone, F. Field investigation of rill and ephemeral gully erosion in the Sparacia experimental area, South Italy. *Catena* **2013**, *101*, 226–234. [CrossRef]
28. Ichim, I.; Mihaiu, G.; Surdeanu, V.; Radoane, M.; Radoane, N. Gully erosion agricultural lands in Romania. In *Soil Erosion on Agricultural Land*; Boardman, J., Foster, D.L., Dearing, J.A., Eds.; Wiley: Hoboken, NJ, USA, 1990; pp. 55–67.
29. Daba, S.; Rieger, W.; Strauss, P. Assessment of gully erosion in eastern Ethiopia using photogrammetric technique. *Catena* **2003**, *50*, 273–291. [CrossRef]
30. Moges, A.; Holden, H.M. Estimating the rate and consequences of gully development, a case study of Umbulo Catchment in southern Ethiopia. *Land. Degrad. Dev.* **2008**, *19*, 574–586. [CrossRef]
31. Vandaele, K. Assessment of factors affecting ephemeral gully erosion in cultivated catchments of the Belgian loam belt. In *Farm Land Erosion in Temperate Plains Environment and Hills*; Elsevier Science Publishers: Amsterdam, The Netherlands, 1993; pp. 125–136.
32. Di Stefano, C.; Ferro, V.; Pampalone, V. Modeling rill erosion at the Sparacia experimental area. *J. Hydrol. Eng.* **2015**, *20*, C5014001. [CrossRef]
33. Natural Resources Conservation Service & Agriculture Department (Ed.) *Keys to Soil Taxonomy: 2010*; Government Printing Office: Washington, DC, USA, 2010.
34. Wischmeier, W.H.; Smith, D.D. *Predicting Rainfall-Erosion Losses—A Guide to Conservation Farming*; USDA Agricultural Handbook No. 537; USDA: Blacksburg, VA, USA, 1978.
35. Carollo, F.G.; Di Stefano, C.; Ferro, V.; Pampalone, V.; Sanzone, F. Testing a new sampler for measuring plot soil loss. *Earth Surf. Process. Landf.* **2016**, *41*, 867–874. [CrossRef]
36. Fiorillo, F.; Limongiello, M.; Fernández-Palacios, B.J. Testing GoPro for 3D model reconstruction in narrow spaces. *Acta Imeko* **2016**, *5*, 64–70. [CrossRef]
37. Seiz, S.M.; Curless, B.; Diebel, J.; Scharstein, D.; Szeliski, R. A comparison and evaluation of multi-view stereo reconstruction algorithms. In Proceedings of the 2006 IEEE Computer Society Conference on Computer Vision and Pattern Recognition (CVPR'06), New York, NY, USA, 17–22 June 2006.
38. Thommeret, N.; Bailly, J.S.; Puech, C. Extraction of thalweg networks from DTMs: Application to badlands. *Hydrol. Earth Syst. Sci.* **2010**, *14*, 1527–1536. [CrossRef]
39. Nicosia, A.; Palmeri, V.; Pampalone, V.; Di Stefano, C.; Ferro, V. Slope threshold in rill flow resistance. *Catena* **2022**, *208*, 105789. [CrossRef]
40. Di Stefano, C.; Nicosia, A.; Palmeri, V.; Pampalone, V.; Ferro, V. Estimating flow resistance in steep slope rills. *Hydrol. Process.* **2021**, *35*, e14296. [CrossRef]
41. Fang, H.; Sun, L.; Tang, Z. Effects of rainfall and slope onrunoff, soil erosion and rill development: An experimental study using two loess soils. *Hydrol. Process.* **2015**, *29*, 2649–2658. [CrossRef]
42. Bagarello, V.; Ferro, V.; Pampalone, V. A new version of theUSLE-MM for predicting bare plot soil loss at the Sparacia (South Italy) experimental site. *Hydrol. Process.* **2015**, *29*, 4210–4219. [CrossRef]
43. Govers, G.; Poesen, J. Assessment of the interrill and rill contribution to total soil loss from an upland field plot. *Geomorphology* **1988**, *1*, 343–354. [CrossRef]